Supplementary Material

Adsorption of toxic gases on borophene: surface deformation links to chemisorptions

Luong Thi Ta[1,2,3], Ikutaro Hamada[1,4], Yoshitada Morikawa[1,4,5] and Van An Dinh*[2,6]*

[1] Department of Precision Engineering, Graduate School of Engineering, Osaka University, 2-1, Yamadaoka, Suita, Osaka 565-0871, Japan.

[2] Nanotechnology Program, VNU Vietnam Japan University, Luu Huu Phuoc Str., My Dinh I, Nam Tu Liem, Hanoi, 100000, Vietnam.

[3] Department of Chemistry, Institute of Environment, Vietnam Maritime University, Le Chan, Haiphong, 18000, Vietnam.

[4] Elements Strategy Initiative for Catalysts and Batteries (ESICB), Kyoto University, Goryo-Ohara, Nishikyo-ku, Kyoto 615-8245, Japan.

[5] Research Center for Ultra-Precision Science and Technology, Graduate School of Engineering, Osaka University, 2-1 Yamadaoka, Suita, Osaka, 565-0871, Japan.

[6] Center for Atomic and Molecular Technologies, Graduate School of Engineering, Osaka University, 2-1 Yamadaoka, Suita, Osaka, 565-0871, Japan.

(*) Corresponding authors: morikawa@prec.eng.osaka-u.ac.jp (Y. Morikawa); dv.an@vju.ac.vn (V. A. Dinh)

Contents

S1. Interaction energy as a function of spatial coordinate

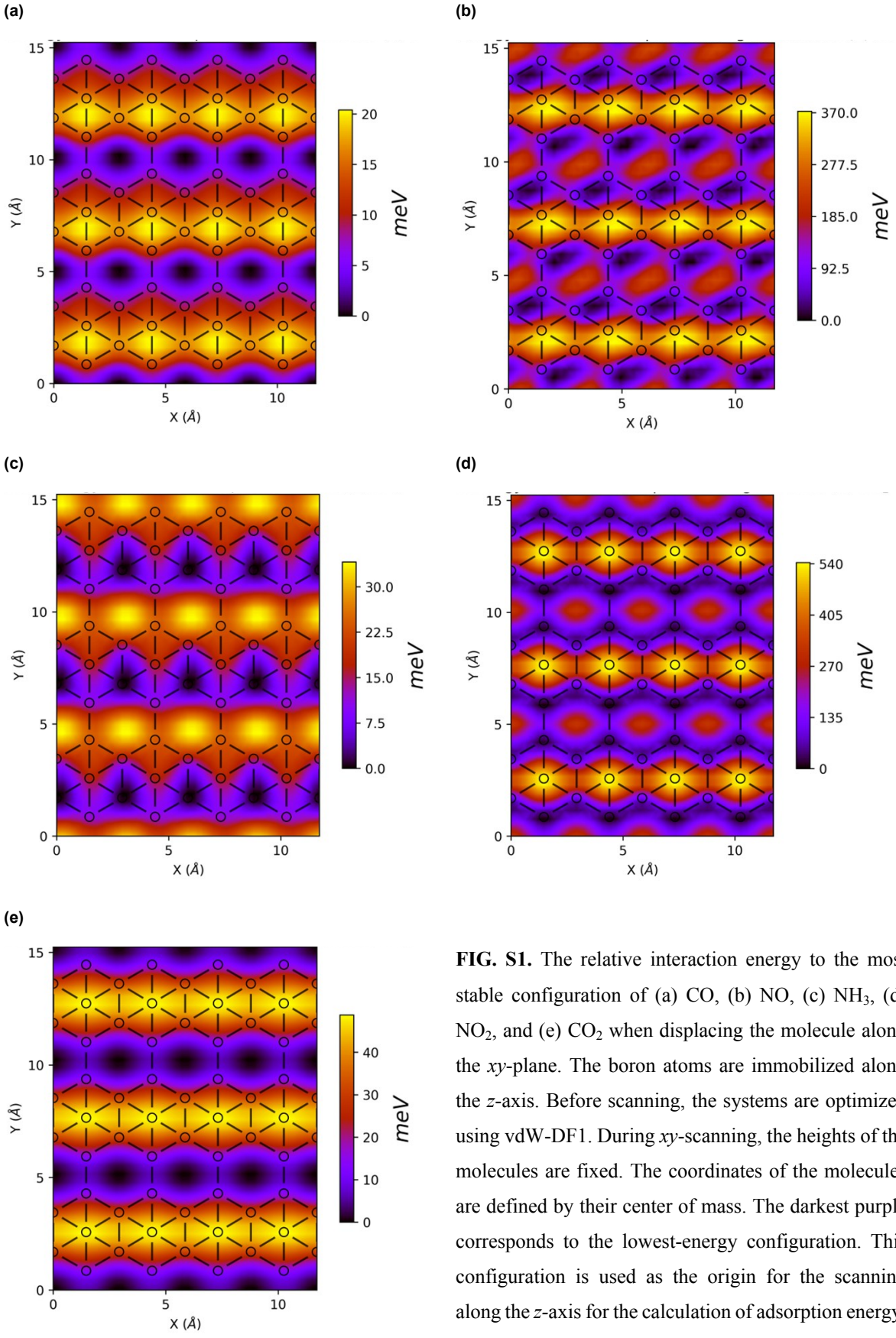

FIG. S1. The relative interaction energy to the most stable configuration of (a) CO, (b) NO, (c) NH_3, (d) NO_2, and (e) CO_2 when displacing the molecule along the *xy*-plane. The boron atoms are immobilized along the *z*-axis. Before scanning, the systems are optimized using vdW-DF1. During *xy*-scanning, the heights of the molecules are fixed. The coordinates of the molecules are defined by their center of mass. The darkest purple corresponds to the lowest-energy configuration. This configuration is used as the origin for the scanning along the *z*-axis for the calculation of adsorption energy.

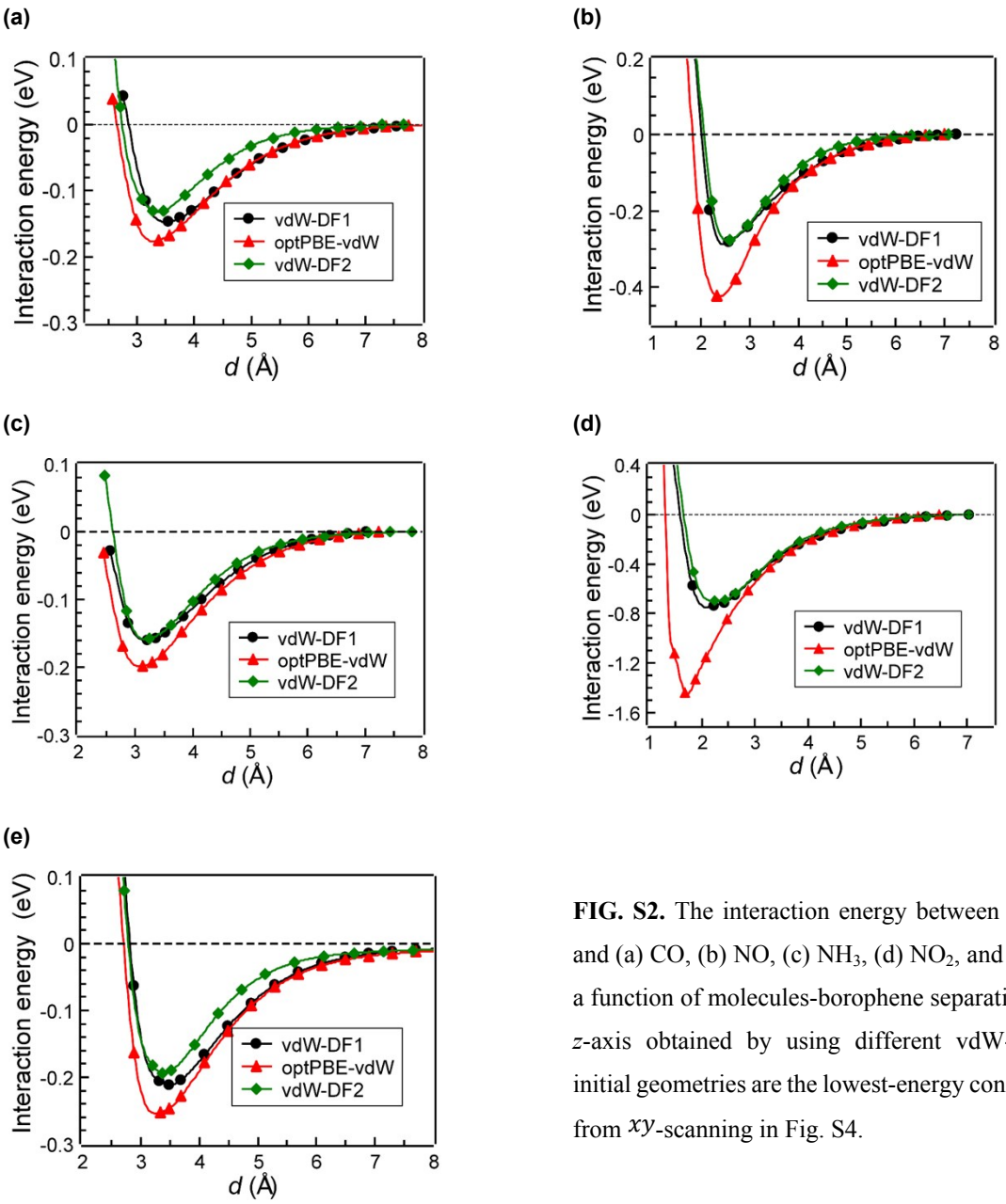

FIG. S2. The interaction energy between borophene and (a) CO, (b) NO, (c) NH_3, (d) NO_2, and (e) CO_2 as a function of molecules-borophene separation d along z-axis obtained by using different vdW-DFs. The initial geometries are the lowest-energy configurations from xy-scanning in Fig. S4.

S2. Gas-phase computational details

All calculations of molecules in the gas phase were carried out using the model of a single molecule in a vacuum box. The box has the same size as that in the adsorption systems. The Gamma k-point was used. The exchange-correlation functional optPBE-vdW was employed for the sake of consistency with the adsorption systems. The other parameters were set as presented in the Computational details section.

Table S1. Summary gas profiles in isolated and adsorption states

	CO		NO		NH_3		NO_2		CO_2	
	Gas-phase	Ads. state	Gas-phase	Ads. state	Gas-phase	Ads. state	Gas-phase	Ads. state	Gas-phase	Ads. state
Bond length	1.14	1.16	1.170	1.186	1.021	1.028	1.216	1.363 1.213	1.177	1.178
Bond angle	-	-	-	-	106.6°	108°	133.4°	120.7°	180°	180°

The unit of bond length is angstrom

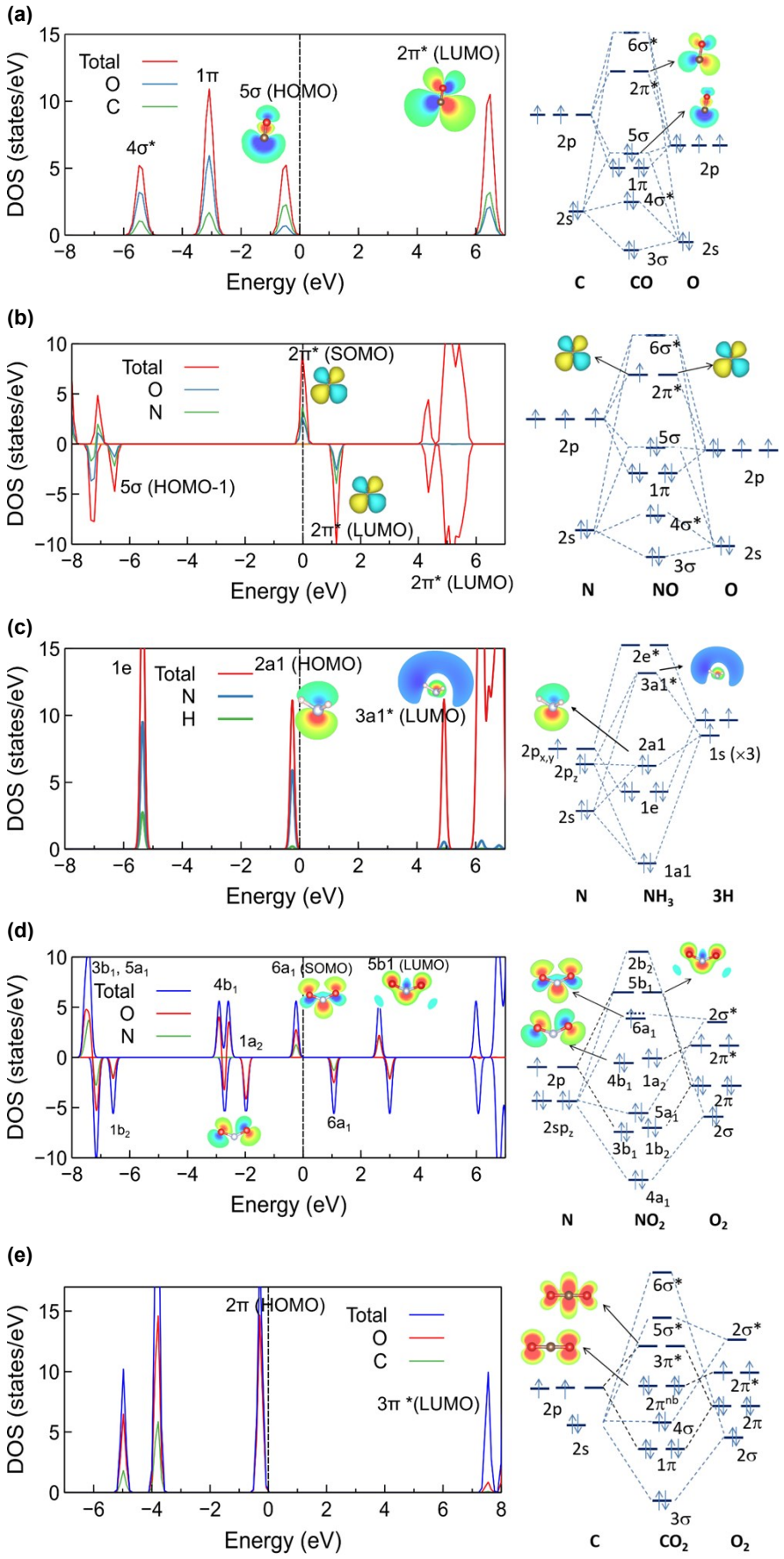

FIG. S3. Electronic structure and molecular orbital diagram of (a) CO, (b) NO, (c) NH_3, (d) NO_2, and (e) CO_2 molecule. Insets are spatial distributions of HOMOs and LUMOs.

S3. Employment of a later generation of non-local vdW-DF: vdW-DF3

Table S2. Adsorption energies (E_{ad}) and adsorption distances (d) of CO_2, CO, NH_3, NO, and NO_2 on borophene obtained using two options of vdW-DF3 functional[1] (i.e., vdW-DF3-opt1 and vdW-DF3-opt2). The calculations were performed using PAW method implemented in Quantum Espresso code. The convergence threshold for self-consistent field calculations was set to 10^{-10} Ry/cell. Convergence threshold on forces acting on atoms for the ionic minimization was set to 5×10^{-4} Ry/borh. The kinetic-energy cutoff was set to 40 Ry. The structure and k-point sampling settings are the same as described in the Methodology section.

Molecules	Adsorption properties	vdW-DF3-opt1	vdW-DF3-opt2
CO_2	E_{ad} (eV)	-0.18	-0.19
	d (Å)	3.21	3.25
CO	E_{ad} (eV)	-1.17	-1.08
	d (Å)	1.48	1.49
NH_3	E_{ad} (eV)	-1.11	-1.03
	d (Å)	1.62	1.63
NO	E_{ad} (eV)	-1.01	-0.91
	d (Å)	1.38	1.38
NO_2	E_{ad} (eV)	-1.95	-1.80
	d (Å)	1.56	1.57

S4. Comparison of borophene to other 2D-materials in adsorption energies

Table S3. Adsorption energies (eV) of CO_2, CO, NH_3, NO, and NO_2 on 2D materials calculated by different vdW functionals

	vdW approx.	borophene		graphene	MoS_2	WS_2	german-ene	phospho-rene
		This work	[2,3]	[4,5]	[6]	[7]	[8]	[9]*
CO_2	vdW-DF1	-0.21	--	-0.38 [c]	-0.21	--	--	--
	optPBE-vdW	-0.27	--	--	-0.25	--	--	--
	vdW-DF2	-0.19	--	--	--	--	--	--
	rev-vdW-DF2	-0.32	--	-0.27 [c]	--	--	--	--
	PBE-D2	--	-0.18 [a]	--	-0.14	--	-0.10	--
CO	vdW-DF1	-0.64	--	--	-0.14	-0.21	--	--
	optPBE-vdW	-0.86	--	--	-0.16	--	--	-0.31
	vdW-DF2	-0.49	--	-0.11 [d]	--	--	--	--
	rev-vdW-DF2	-1.18	--	--	--	--	--	--
	PBE-D2	--	-1.19 [b]	--	-0.07	-0.11	-0.16	--
NH_3	vdW-DF1	-0.52	--	--	-0.13	--	--	--
	optPBE-vdW	-0.83	--	--	-0.18	--	--	-0.18
	vdW-DF2	-0.41	--	-0.10 [d]	--	--	--	--
	rev-vdW-DF2	-1.15	--	--	--	--	--	--
	PBE-D2	--	-1.11 [b]	--	-0.13	--	-0.44	--
NO	vdW-DF1	-0.39	--	--	-0.24	--	--	--
	optPBE-vdW	-0.72	--	--	-0.25	-0.25	--	-0.32
	vdW-DF2	-0.38	--	--	--	--	--	--
	rev-vdW-DF2	-1.05	--	--	--	--	--	--
	PBE-D2	--	-0.95 [b]	--	-0.15	-0.13	-0.51	--
NO_2	vdW-DF1	-1.56	--	--	-0.24	--	--	--
	optPBE-vdW	-1.67	--	--	-0.29	--	--	-0.50
	vdW-DF2	-1.28	--	-0.18 [d]	--	--	--	--
	rev-vdW-DF2	-1.91	--	--	--	--	--	--
	PBE-D2	--	-1.80 [b]	--	-0.14	--	-1.08 [g]	--

[a] Ref. [2]; [b] Ref. [3]; [c] Ref. [4]; [d] Ref. [5];

* In ref [9], the functional optB88-vdW was used.

S5. Vibration modes of molecules in the gas phase and adsorption state

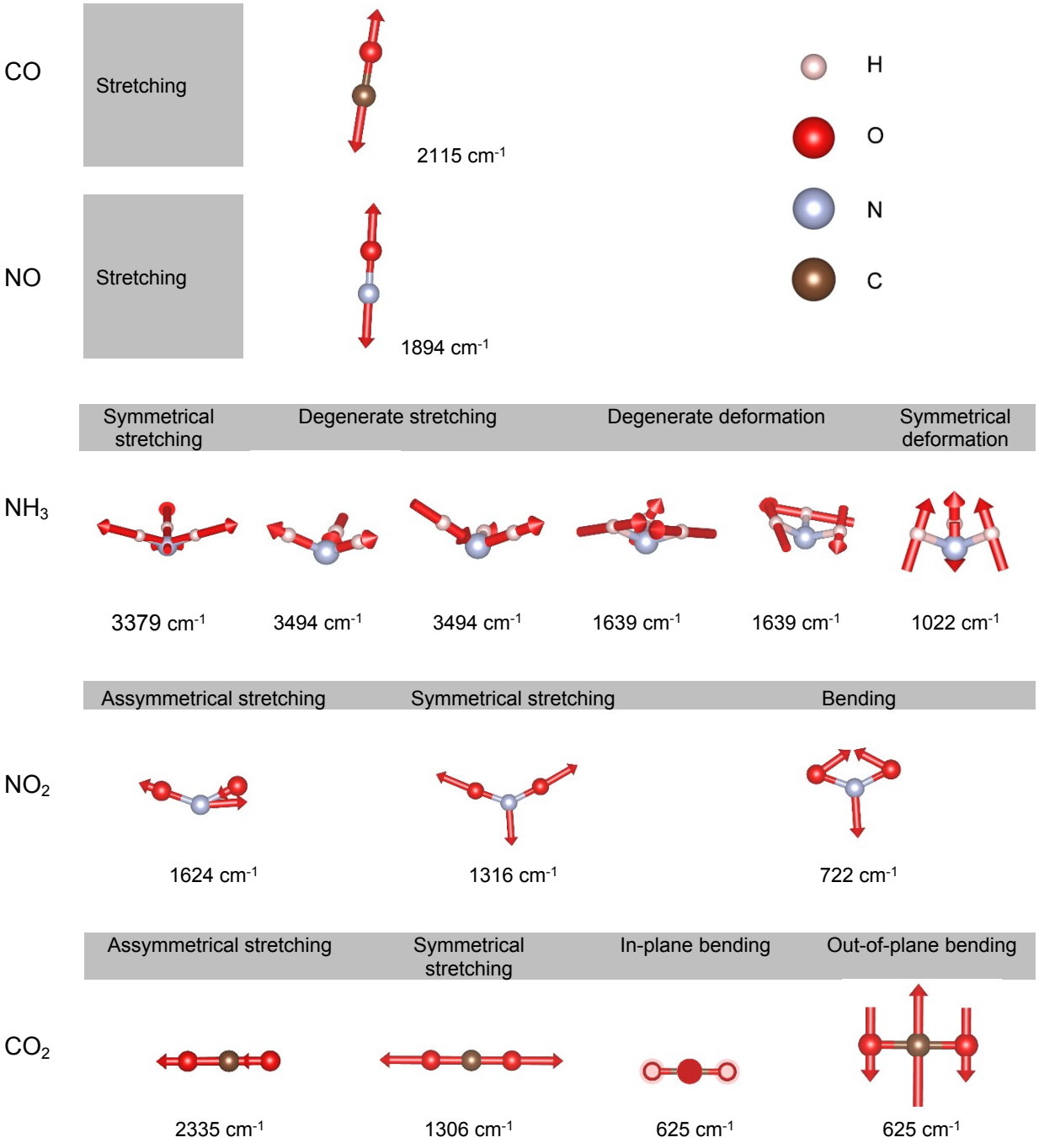

FIG. S4. Vibrational modes of CO, NO, NH_3, NO_2, and CO_2 in the gas phase.

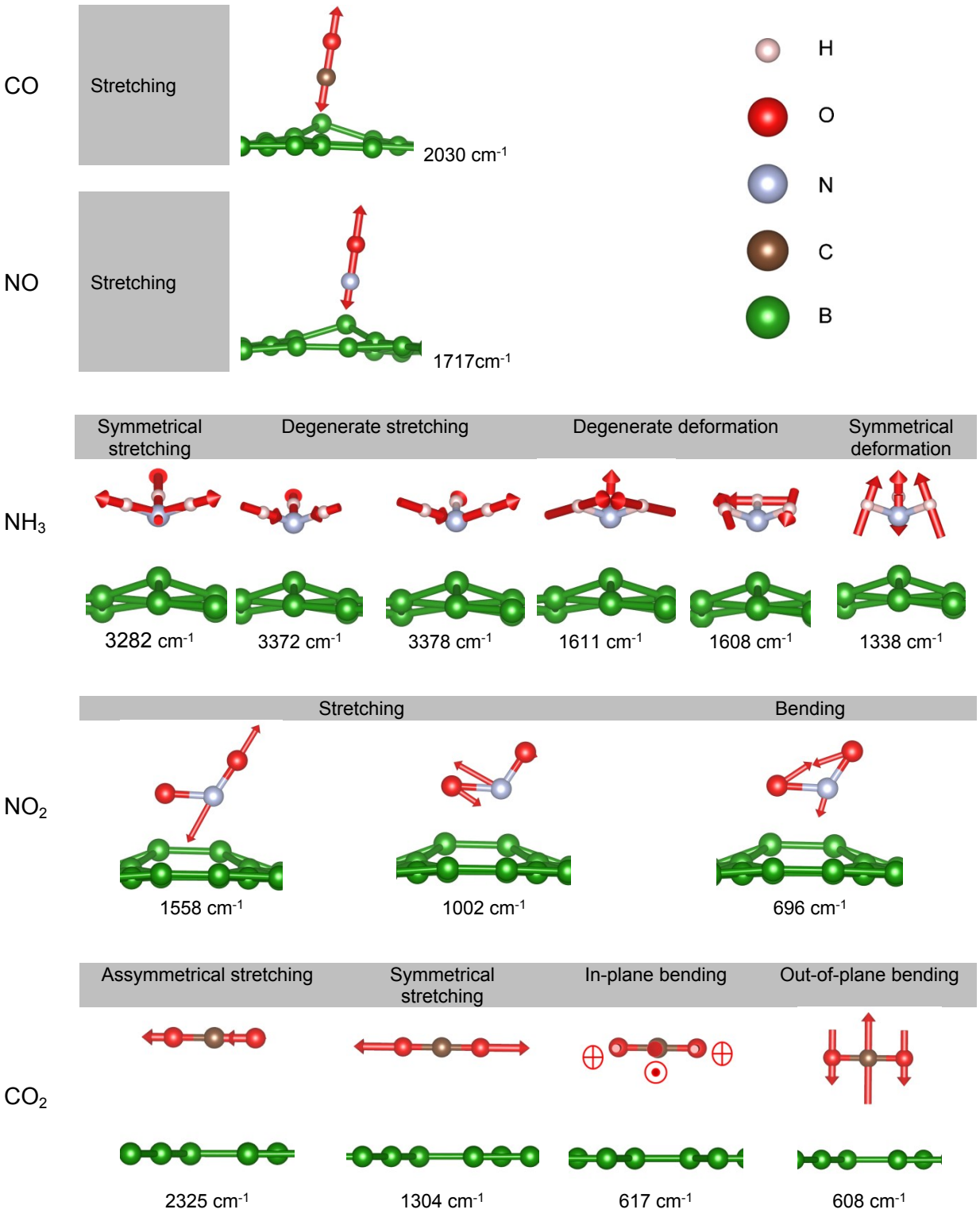

FIG. S5. Vibrational modes of CO, NO, NH_3, NO_2, and CO_2 in adsorption state.

S6. Explanation of softening vibrational modes

We investigated the bonding between C and O in the CO molecule after adsorption. The 5σ donation and $2\pi^*$ backdonation induce the weakening of the C − O bond due to the partially filled $2\pi^*$ with the antibonding character. This is supported by the COOP analysis between AOs of C and O atoms. As seen in Fig. S6, negative COOP develops from $E_F - 4$ eV, where the antibonding $2\pi^*$ orbital of CO is partially occupied, leading to weakening of the C − O bond as well as softening of the CO stretching mode (Fig. S4 and S5).

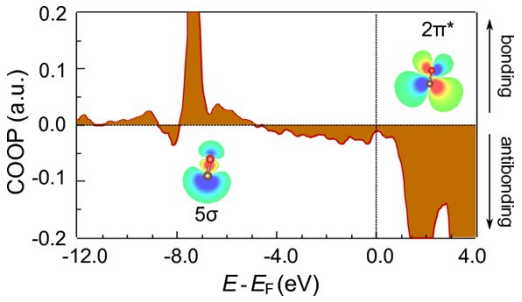

FIG. S6. Crystal orbital overlap population (COOP) between atomic orbitals of C and O atoms for CO chemisorbed on borophene. Insets show HOMO (5σ) and LUMO ($2\pi^*$) of CO.

The calculated vibrational frequencies of gas-phase NO_2 are 1624, 1316, and 722 cm^{-1} corresponding to the experimentally measured 1618 cm^{-1} (asymmetrical stretching), 1318 cm^{-1} (symmetrical stretching), and 750 cm^{-1} (bending modes) [10], respectively. Due to the strong interaction with borophene, these frequencies are significantly red-shifted to 1558, 1002, and 696 cm^{-1} accordingly (Fig. S4 and S5). The softening of these vibrational modes of gases can be also explained by COOP analysis regarding N-O bonds in the adsorption state, as shown in Fig. S7. It is found that the $6a_1$ orbital hybridizes with the $1a_2$, and the antibonding states are partially occupied in the adsorption state. This leads to the weakening and elongation of the N-O bond, thereby softening the vibrational modes of the NO_2 molecule.

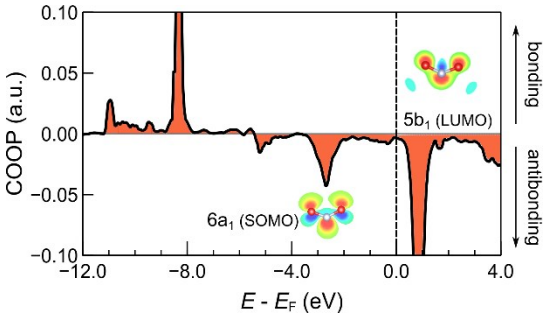

FIG. S7. Crystal orbital overlap population (COOP) between atomic orbitals of N and O atoms of NO_2 in the adsorption state.

S7. Electronic analyses of NO and CO_2 interacting with borophene

NO

To gain insight into the interaction between NO and borophene, we calculated COOP and PDOS onto MOs of NO (Fig. S8). Thereby, NO becomes spin unpolarized upon adsorption because of the strong hybridization of its $2\pi^*$ frontier orbitals and borophene states.

COOP and PDOS reveal that the model of 5σ donation and $2\pi^*$ backdonation is appropriate for NO – borophene chemisorption, similar to CO (Fig. S8a,b). The 5σ, 1π, and filled $2\pi^*$ orbitals contribute to the bonding states, but the contribution of $2\pi^*$ in this case, is greater. Note that both 5σ and $2\pi^*$ orbitals are significantly delocalized. The 5σ states consecutively distribute from ca. -10 eV to more than $+4$ eV with respect to E_F. Similarly, $2\pi^*$ states distribute ranging from $E_F - 9$ eV to $E_F + 4$ eV. The great delocalization implies that these orbitals strongly interact with the surface. Considering the intermolecular B – NO bond (Fig. S8c), we found that bonding between NO and B are attributed mostly to 1π - $2p_{xy}$, and $2\pi^*$ - $2p_{xy}$ interactions.

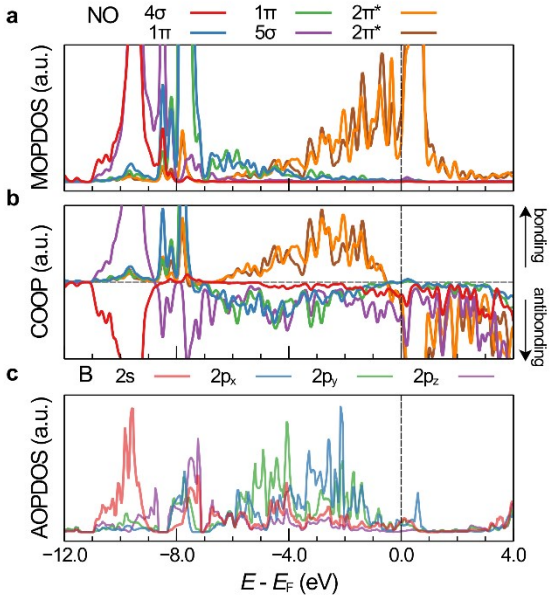

FIG. S8. (a) Molecular-orbital projected density of states (MOPDOS) of NO on borophene. (b) Crystal orbital overlap population (COOP) between NO and borophene. (c) Atomic-orbital projected density of states (AOPDOS) of the nearest neighbor B atom to NO.

The calculated charge density difference is shown in Fig. S9. There is charge accumulation corresponding to the backdonation to $2\pi^*$ orbital and to the bond formation between B and O. Meanwhile the charge depletion is owing to the donation of 5σ orbital. This charge rearrangement is similar to that in the CO/borophene system.

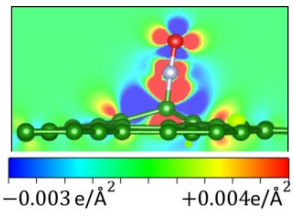

FIG. S9. Charge density difference induced by the adsorption of NO on borophene.

CO_2

By inspecting the electronic structure shown in Fig. S10, we found that CO_2 does not experience a significant change in its electronic structure; all peaks remain localized at the same positions. However, the $3\pi^*$ orbital (LUMO) is partially occupied. This is reflected in the charge density difference (Fig. S11), in which the electron accumulation can be seen in the vicinity of O.

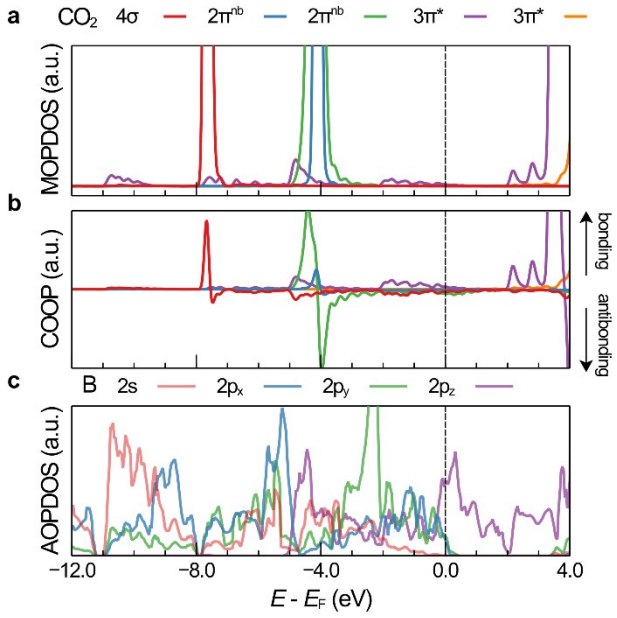

FIG. S10. (a) Molecular-orbital projected density of states (MOPDOS) of CO_2 on borophene. (b) Crystal orbital overlap population (COOP) between CO_2 and borophene. (c) Atomic-orbital projected density of states (AOPDOS) of nearest neighbor B atom of CO_2.

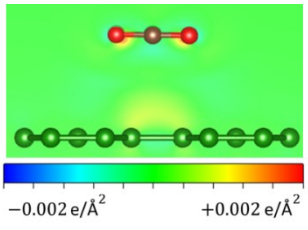

FIG. S11. Charge density difference of CO_2^- borophene induced by the adsorption.

References

1 D. Chakraborty, K. Berland and T. Thonhauser, *J. Chem. Theory Comput.*, 2020, **16**, 5893–5911.

2 X. Tan, H. A. Tahini and S. C. Smith, *ACS Appl. Mater. Interfaces*, 2017, **9**, 19825–19830.

3 C. S. Huang, A. Murat, V. Babar, E. Montes and U. Schwingenschlögl, *J. Phys. Chem. C*, 2018, **122**, 14665–14670.

4 K. Takeuchi, S. Yamamoto, Y. Hamamoto, Y. Shiozawa, K. Tashima, H. Fukidome, T. Koitaya, K. Mukai, S. Yoshimoto, M. Suemitsu, Y. Morikawa, J. Yoshinobu and I. Matsuda, *J. Phys. Chem. C*, 2017, **121**, 2807–2814.

5 X. Lin, J. Ni and C. Fang, *J. Appl. Phys.*, 2013, **113**, 034306.

6 S. Zhao, J. Xue and W. Kang, *Chem. Phys. Lett.*, 2014, **595–596**, 35–42.

7 V. Q. Bui, T.-T. Pham, D. A. Le, C. M. Thi and H. M. Le, *J. Phys. Condens. Matter*, 2015, **27**, 305005.

8 W. Xia, W. Hu, Z. Li and J. Yang, *Phys. Chem. Chem. Phys.*, 2014, **16**, 22495–22498.

9 Y. Cai, Q. Ke, G. Zhang and Y.-W. Zhang, *J. Phys. Chem. C*, 2015, **119**, 3102–3110.

10 T. Shimanouchi, *J. Phys. Chem. Ref. Data*, 1977, **6**, 993–1102.